



Computational fluid dynamics analysis of a twisted airfoil shaped two-bladed H-Darrieus rotor made from fibreglass reinforced plastic (FRP)

Rajat Gupta, Sukanta Roy, Agnimitra Biswas

Department of Mechanical Engineering, National Institute of Technology, Silchar, Assam, 788010 India.

Abstract

H-Darrieus rotor is a lift type device having two to three blades designed as airfoils. The blades are attached vertically to the central shaft through support arms. The support to vertical axis helps the rotor maintain its shape. In this paper, Computational Fluid Dynamics (CFD) analysis of an airfoil shaped two-bladed H-Darrieus rotor using Fluent 6.2 software was performed. Based on the CFD results, a comparative study between experimental and computational works was carried out. The H-Darrieus rotor was 20cm in height, 5cm in chord and twisted with an angle of 30° at the trailing end. The blade material of rotor was Fiberglass Reinforced Plastic (FRP). The experiments were earlier conducted in a subsonic wind tunnel for various height-to-diameter (H/D) ratios. A two dimensional computational modeling was done with the help of Gambit tool using unstructured grid. Realistic boundary conditions were provided for the model to have synchronization with the experimental conditions. Two dimensional steady-state segregated solver with absolute velocity formulation and cell based grid was considered, and a standard k- ϵ viscous model with standard wall functions was chosen. A first order upwind discretization scheme was adopted for pressure velocity coupling of the flow. The inlet velocities and rotor rotational speeds were taken from the experimental results. From the computational analysis, power coefficient (C_p) and torque coefficient (C_t) values at ten different H/D ratios namely 0.85, 1.0, 1.10, 1.33, 1.54, 1.72, 1.80, 1.92, 2.10 and 2.20 were calculated in order to predict the performances of the twisted H-rotor. The variations of C_p and C_t with tip speed ratios were analyzed and compared with the experimental results. The standard deviations of computational C_p and C_t from experimental C_p and C_t were obtained. From the computational analysis, the highest values of C_p and C_t were obtained at H/D ratios of 1.0 and 1.54 respectively. The deviation of computational C_p from experimental C_p was within $\pm 2.68\%$. The deviation of computational C_t from experimental C_t was within $\pm 3.66\%$. Thus, the comparison between computational works and experimental works is quite encouraging.

Copyright © 2010 International Energy and Environment Foundation - All rights reserved.

Keywords: Computational fluid dynamics, H-Darrieus rotor, Power coefficient, Torque coefficient, Tip speed ratio.

1. Introduction

H-Darrieus rotors are lifting type vertical axis wind machines. These have several advantages over horizontal axis wind machines, like self-starting, inexpensive, omni-directional, single moving part having less balancing problems, facility to place the generator & gear box on ground etc. But the prediction of their behavior is more complex than the horizontal axis turbines [1]. Darrieus wind rotor

was originally invented and patented by G.J.M Darrieus, a French aeronautical engineer, in the year of 1931. Two types of Darrieus rotors are mainly available, namely tropic skein (Eggbeater) Darrieus rotor and H-Darrieus rotor. H-Darrieus rotor was in the same patent of 1931[2]. It has two to three airfoil shaped blades which are attached vertically to the central shaft through support arms as shown in the Figure 1. The support to vertical axis helps the rotor maintain its shape. It is self-regulating in all wind speeds reaching its optimal rotational speed shortly after its cut-in wind speed [3]. Between Seventies and the present decade, many researchers [4-10] had worked on different designs of Savonius rotor to evaluate its maximum attainable efficiency. They showed that the efficiency lies in the range 15% to 38%. However, only few works on H-Darrieus rotor were reported in the literature. Considerable improvement in the understanding of VAWT can be achieved through the use of Computational Fluid Dynamics and experimental measurements [11]. The objective of the present study is to analyze the performance of an airfoil shaped H-Darrieus rotor computationally with the help of Fluent 6.2 software for different height-to-diameter ratios namely 0.85, 1.0, 1.10, 1.33, 1.54, 1.72, 1.80, 1.92, 2.10 and 2.20. The variations of power coefficient (C_p) and torque coefficient (C_t) with tip speed ratio are obtained for each H/D ratio using CFD. Then, the computational results are compared with the experimental results and the standard deviations of computational results from experimental results are found out.



Figure 1. H-Darrieus wind rotor

2. Experimental procedure

The H-Darrieus rotor was 20cm in height and 5cm in chord. It was twisted with an angle of 30° at the trailing end to make it self-starting from no load condition. Rotor blades were made of Fiberglass Reinforced Plastic (FRP). The FRP used was a composite made from polyvinyl chloride (PVC) type thermoplastic reinforced in fine glassfibres. Blade thickness was 5 mm. The experiments for the aforementioned H-rotor were conducted in an open circuit subsonic wind tunnel (Figure 2) for various H/D ratios namely 0.85, 1.0, 1.10, 1.33, 1.54, 1.72, 1.80, 1.92, 2.10 and 2.20. The blades of the model had the provision for change of H/D ratios using nuts and bolts. The cross-sectional area of the wind tunnel test section was 30 cm x 30 cm of length 3 meters. The description of the wind tunnel is available in the literature of Gupta et al. [12]. The air velocity was adjustable between 0-35 m/s.

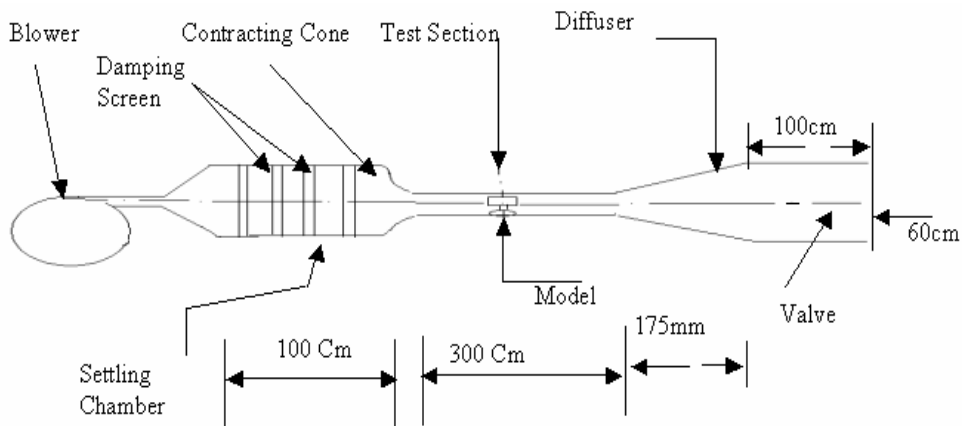


Figure 2. Schematic diagram of subsonic wind tunnel

3. Computational methodology

The computational fluid dynamic code used was fluent while the mesh was generated using gambit. Figure 3 shows the computational domain, which has the two-bladed rotor along with surrounding four edges resembling the test section of the wind tunnel. Realistic boundary conditions are provided for the model to have synchronization with the actual model. Velocity inlet and outflow conditions were taken on the left and right boundaries respectively. The top and bottom boundaries, which signify the sidewalls of the wind tunnel, had symmetry conditions on them. The blades, shaft and the support arms were set to standard wall conditions. Two-dimensional unstructured computational domain was developed with triangular mesh. 17874 nodes and 35262 cells are taken for this model. 18 two-dimensional outflow faces and 18 velocity inlet faces are given. Steady state segregated solver with absolute velocity formulation and cell-based grid was considered, and a standard k- ϵ viscous model with standard wall functions was chosen. A first order upwind discretization scheme was adopted for pressure velocity coupling of the flow. The vertical axis wind turbine blades rotate in the same plane as the approaching wind. For an H-rotor, the general geometric properties of the blade cross-section are usually constant with varying span section unlike Darrieus rotor, for which these geometric properties vary with the local radius. The computational mesh around the rotor is shown in Figure 4.

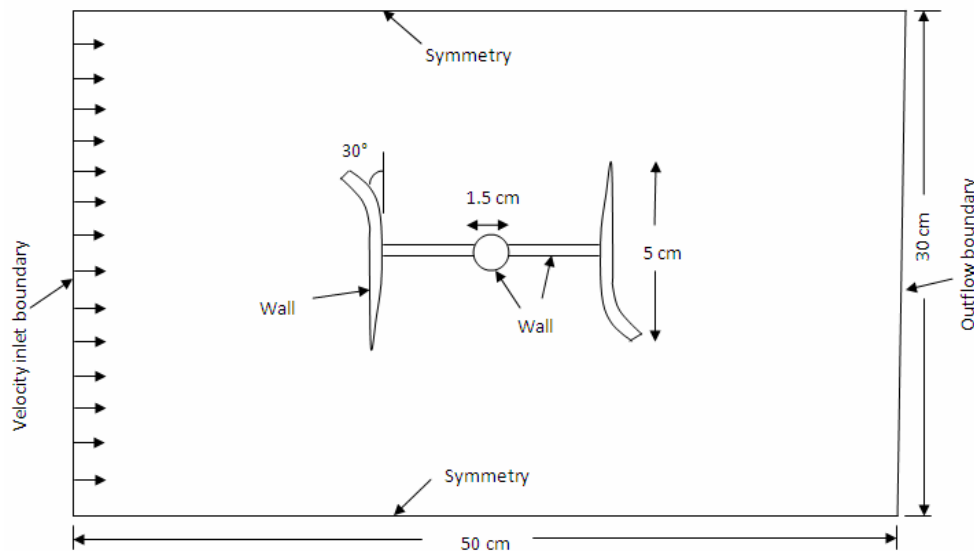


Figure 3. Physical model, boundary conditions and computational domain of 2-bladed H-Darrieus rotor

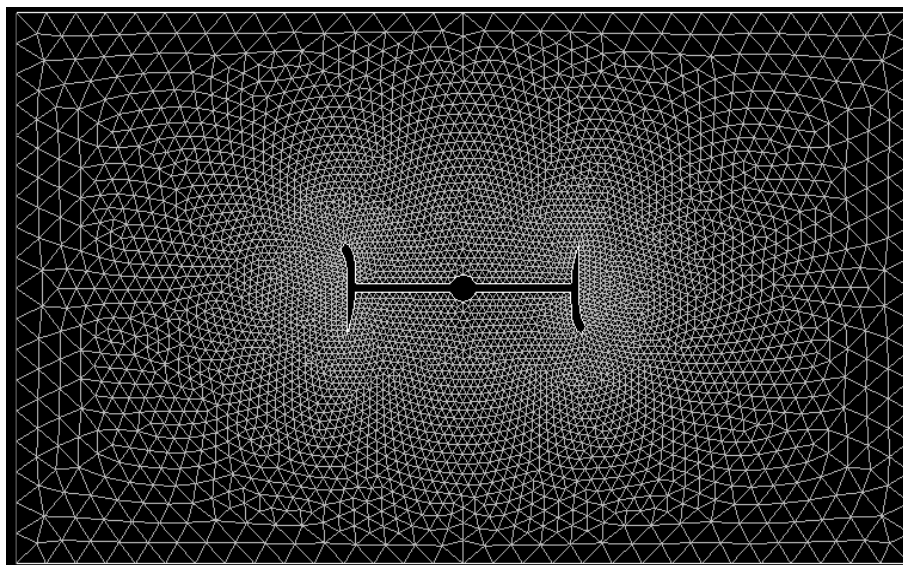


Figure 4. Computational domain after discretization of the Figure 3

3.1 Grid independence test

The computations were initially carried out with various levels of refinement of mesh. The correctness of the result greatly depends upon the resolution of the grid. But, we can refine the grid density up to a certain limit beyond which, refinement does not effect significantly on the result obtained. This limit is called the Grid Independent Limit (GIL). The resolution of the mesh at all important areas was varied in an attempt to reach grid independent limit mesh. In this typical analysis, coefficient of drag (C_d) is taken as the criteria for the test, and the grid refinement is done until the required steady value is not obtained. The various levels of refining used to conduct this study are shown in Table 1. Each level was solved in Fluent with the same set of input parameters. Figure 5 shows the variation of C_d with the no. of nodes, taken in the Grid Independence Test. The refinement level 7 was considered for the final simulation.

Table 1. Nodes and cells used to find GIL for 2 bladed H-rotor

Refined level	No. of Nodes	No. of Cells
1	4616	8976
2	5116	9944
3	7282	14180
4	12782	25126
5	16355	32200
6	17874	35262
7	20597	40612
8	22273	44006
9	24068	48152
10	27424	54074

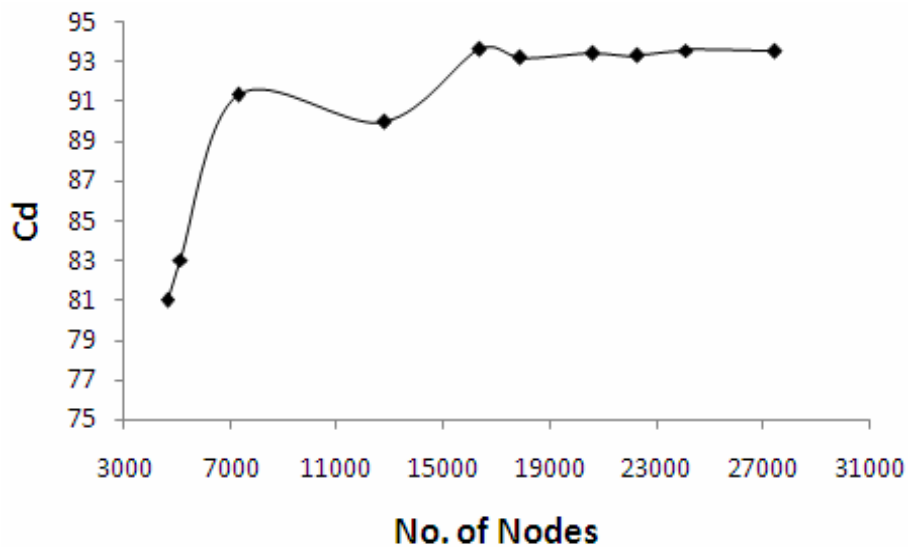


Figure 5. Grid Independence test for 2 bladed H-rotor

3.2 Solution methodology

The input wind velocity and rotor rotational speeds are taken from the earlier experiments done in the department at NIT, Silchar. Appropriate solver, viscous model, material properties, realistic boundary conditions and solution controls provided for this problem are given in Table 2.

Table 2. Solution specifications, boundary conditions and solution controls

Solution Specification	Solver: two dimensional Steady, segregated turbulent (k- ϵ) model with standard wall function and absolute velocity formulation Material: Air ($\rho = 1.225 \text{ Kg/m}^3$, $\mu = 1.7894 \times 10^{-5} \text{ Kg/ms}$) Operating Condition: Atmospheric pressure (1.0132 bar)
Boundary Conditions	Inlet: Velocity inlet Sides: Symmetry, Blades: Wall Outlet: Outflow
Solution Controls	Pressure Velocity Coupling: Simple Under Relaxation Factor: 0.7 (Momentum) Discretization: Momentum (First Order Upwind) Initialization: Inlet condition

4. Results and analysis

After the convergence of the solution, the torque co-efficient (C_t) values are calculated for each value of input air velocity and rotor rotational speed and from the values of C_t , C_p values are obtained by using the following equations [13].

$$C_p = \frac{T}{\frac{1}{2} \rho A V_{free}^3 D} \quad (1)$$

$$C_t = \frac{T}{\frac{1}{2} \rho A V_{free}^2} \quad (2)$$

$$C_p = \frac{1}{2} C_t \frac{D \omega}{V_{free}} \quad (3)$$

$$\lambda = \frac{\pi D N}{60 V_{free}} \quad (4)$$

where C_p is the power coefficient, C_t is the torque coefficient, ρ is the density (kg/m^3), T is the torque (N-m), A is the cross-sectional area (m^2), V_{free} is the free stream velocity (m/s), N is the rotor speed (rpm), D is the overall diameter (m), ω is the angular velocity (rev/sec).

Now the variations of C_p and C_t with Tip speed ratio (λ) are obtained from the CFD results for each H/D ratio, and the computational results are compared with the experimental results. Finally, the standard deviations of the computational results from experimental results are also found out by using the following equations.

$$\sigma = \sqrt{\frac{\sum_{i=1}^n (C_{p_i} - \bar{C}_p)^2}{n-1}} \quad (5)$$

$$\bar{C}_p = \sum_{i=1}^n \frac{C_{p_i}}{n} \quad (6)$$

where σ is the standard deviation, n is the number of data taken.

Now the experimental and computational C_p and C_t with respect to tip speed ratio and the percentage deviations of the computational results from the experimental results for various H/D ratios are shown in Figure 6 to Figure 25.

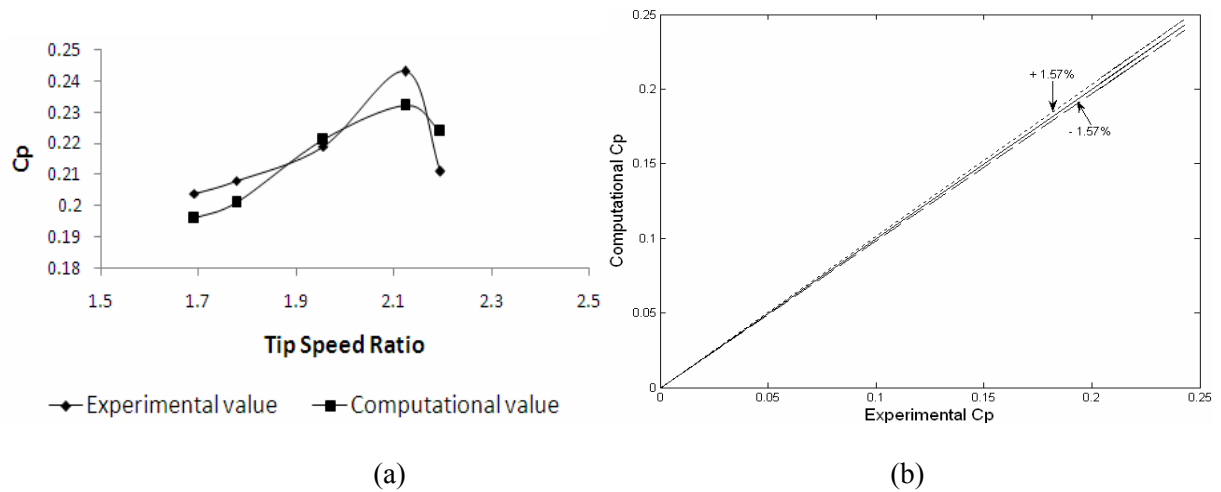


Figure 6. (a) Variation of C_p with TSR, and (b) deviation of computational C_p from experimental C_p for H/D ratio 0.85

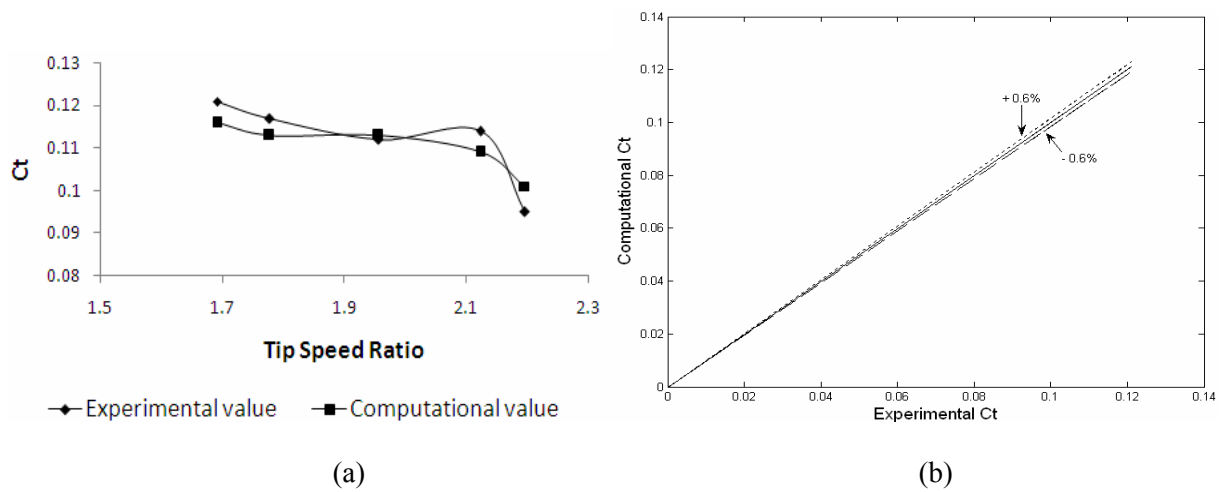


Figure 7. (a) Variation of C_t with TSR, and (b) deviation of computational C_t from experimental C_p for H/D ratio 0.85

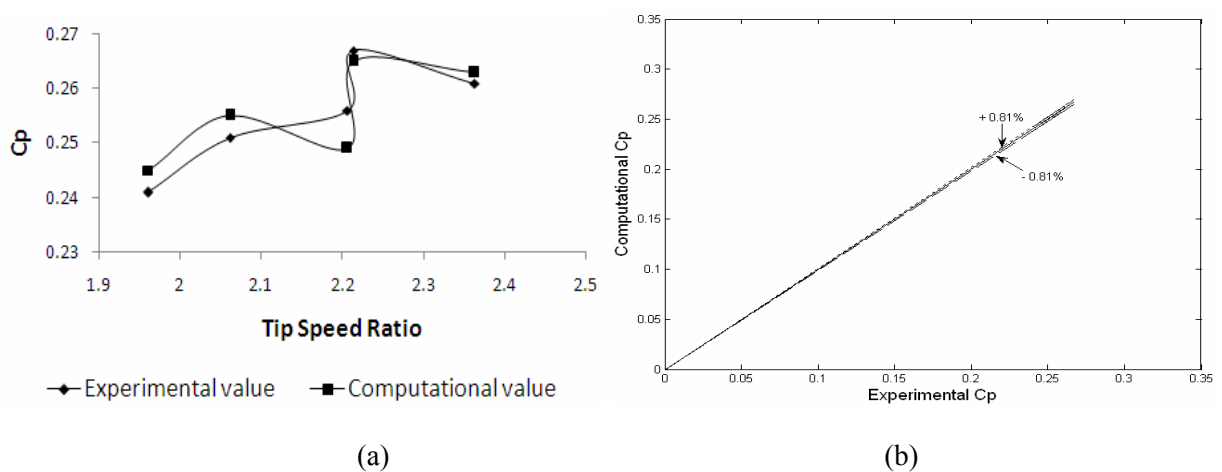


Figure 8. (a) Variation of C_p with TSR, and (b) deviation of computational C_p from experimental C_p for H/D ratio 1.0

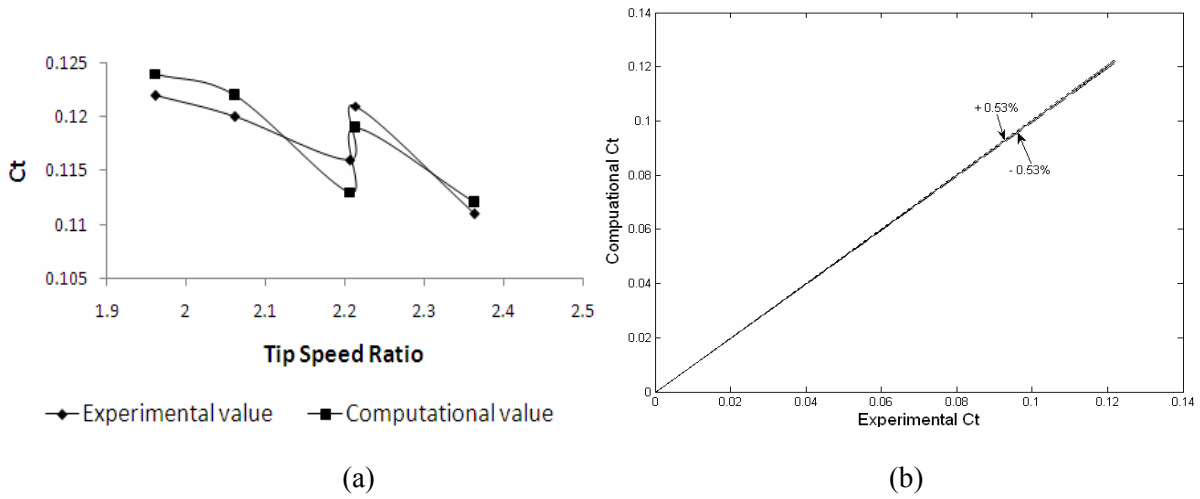


Figure 9. (a) Variation of C_t with TSR, and (b) deviation of computational C_t from experimental C_p for H/D ratio 1.0

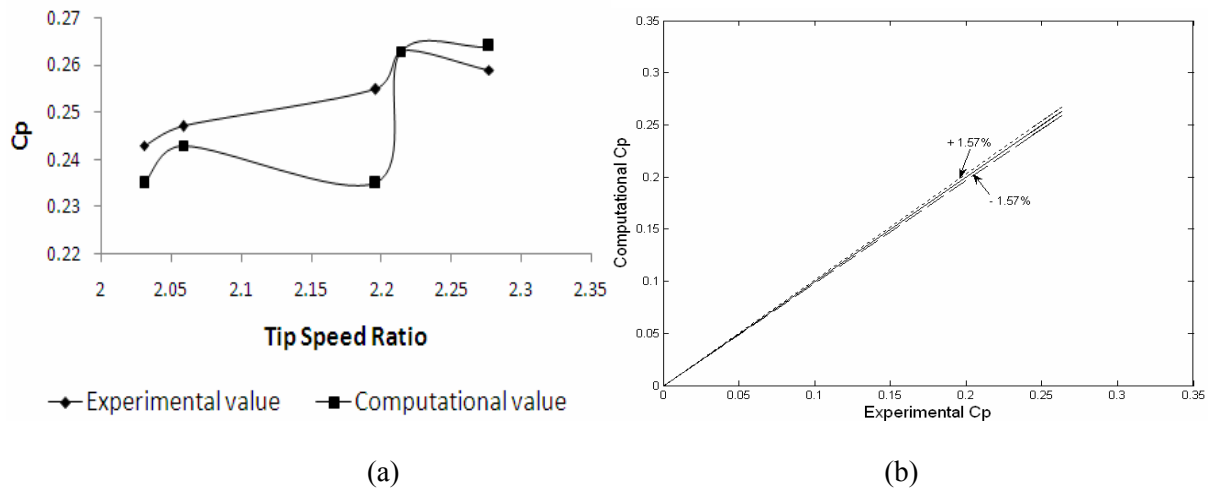


Figure 10. (a) Variation of C_p with TSR, and (b) deviation of computational C_p from experimental C_p for H/D ratio 1.10

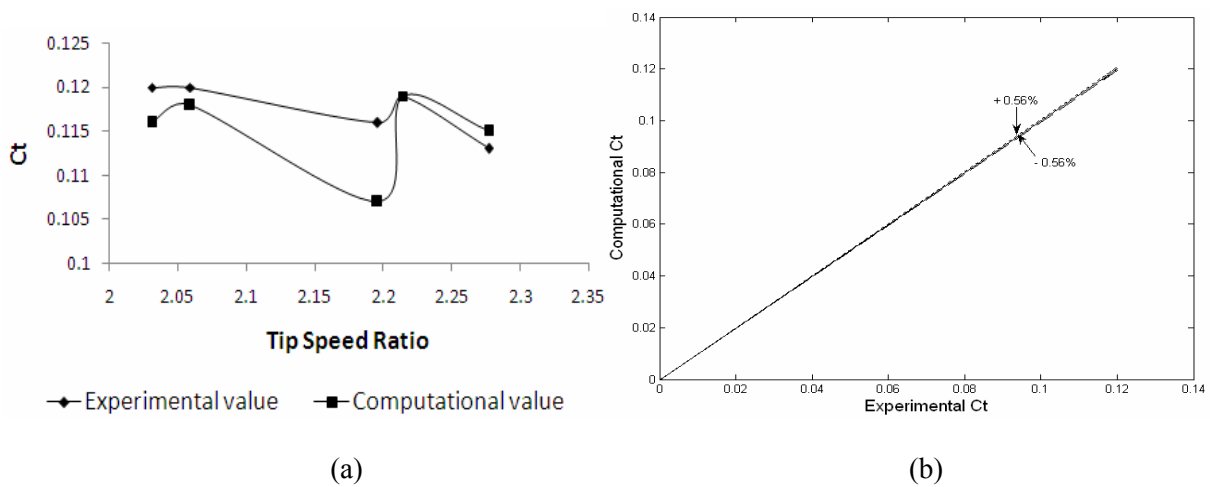


Figure 11. (a) Variation of C_t with TSR, and (b) deviation of computational C_t from experimental C_p for H/D ratio 1.10

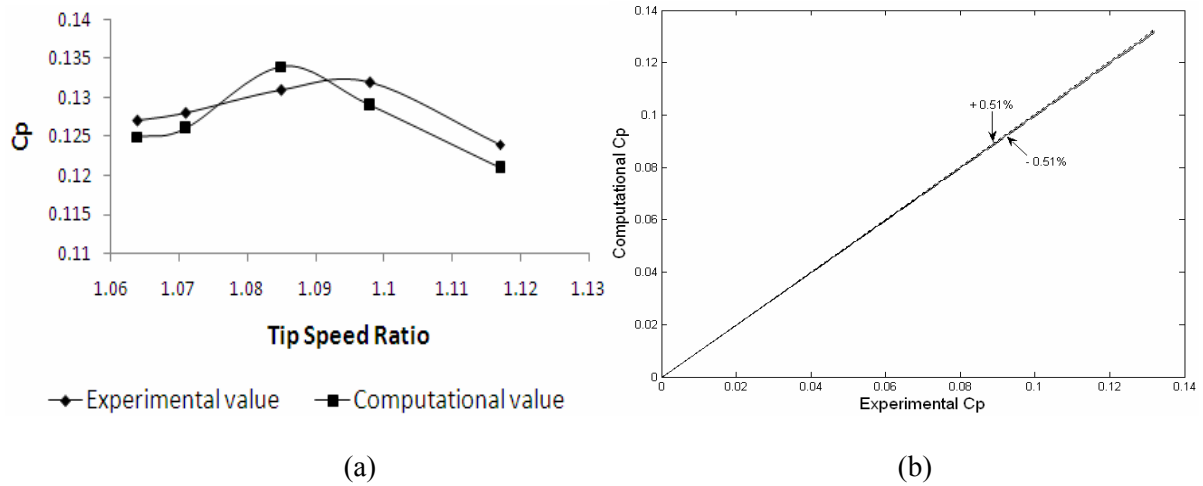


Figure 12. (a) Variation of C_p with TSR, (b) deviation of computational C_p from experimental C_p for H/D ratio 1.33

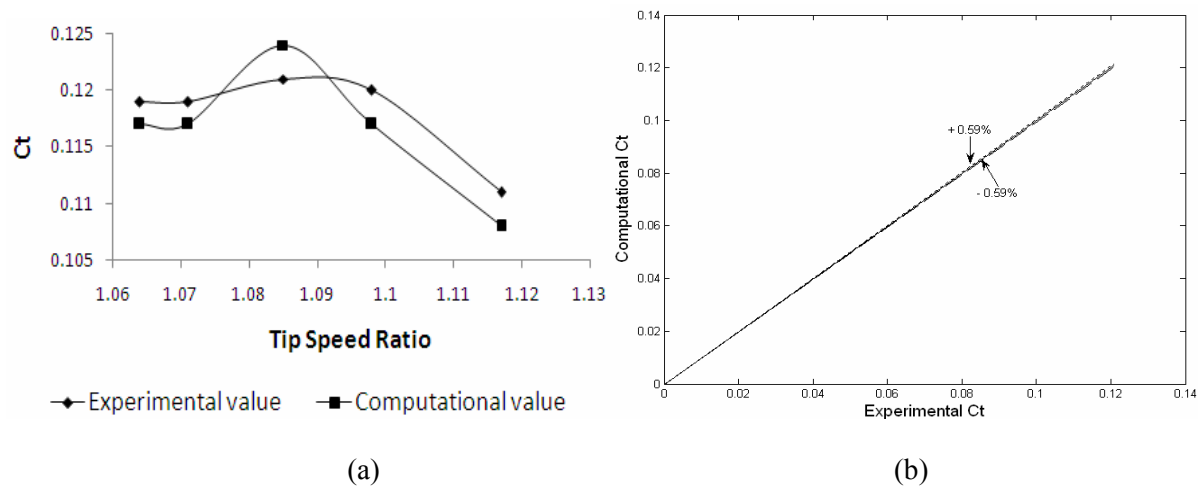


Figure 13. (a) Variation of C_t with TSR, (b) deviation of computational C_t from experimental C_p for H/D ratio 1.33

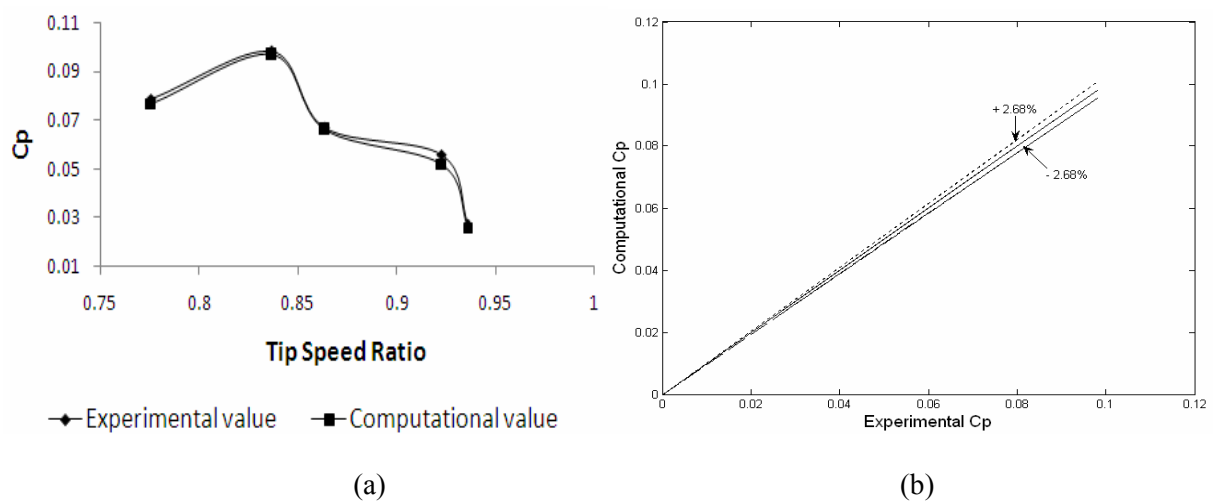


Figure 14. (a) Variation of C_p with TSR, (b) deviation of computational C_p from experimental C_p for H/D ratio 1.54

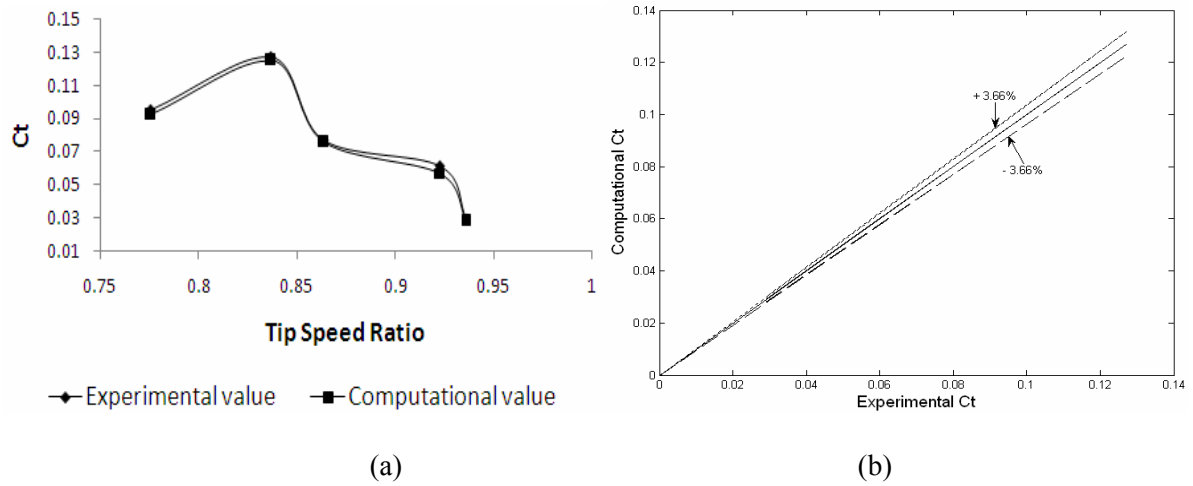


Figure 15. (a) Variation of C_t with TSR, and (b) deviation of computational C_t from experimental C_p for H/D ratio 1.54

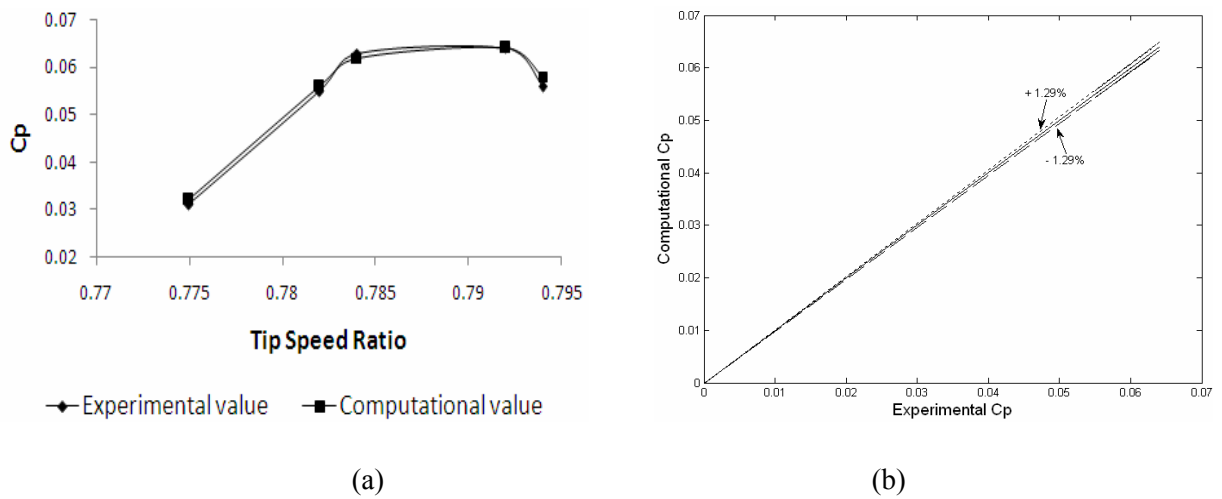


Figure 16. (a) Variation of C_p with TSR, and (b) deviation of computational C_p from experimental C_p for H/D ratio 1.72

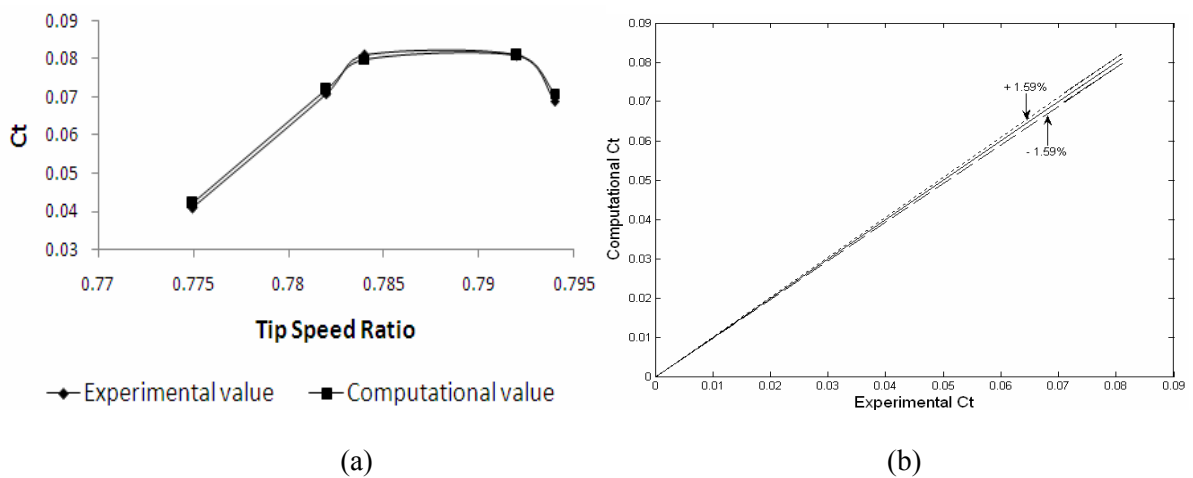


Figure 17. (a) Variation of C_t with TSR, and (b) deviation of computational C_t from experimental C_p for H/D ratio 1.72

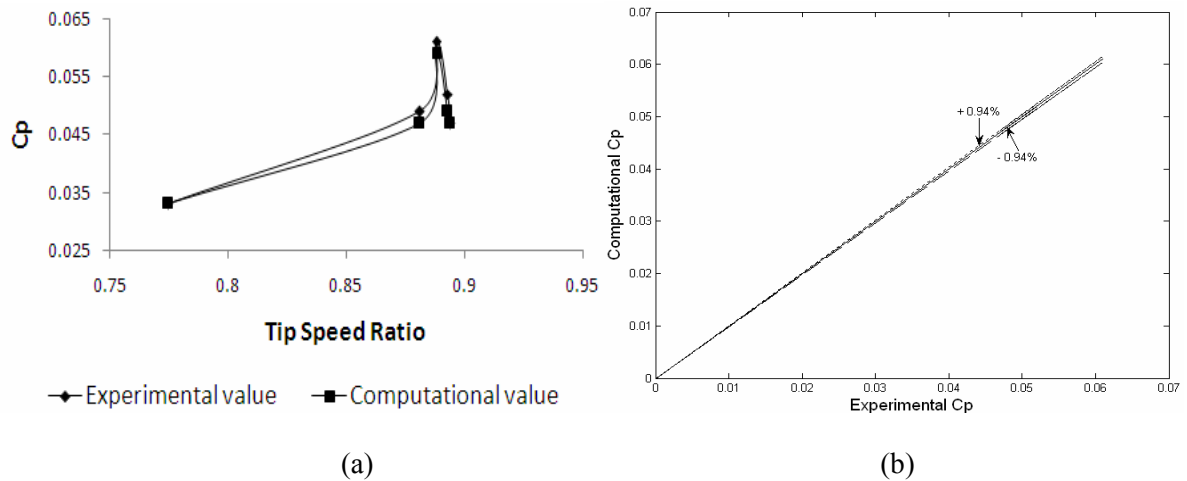


Figure 18. (a) Variation of C_p with TSR, and (b) deviation of computational C_p from experimental C_p for H/D ratio 1.80

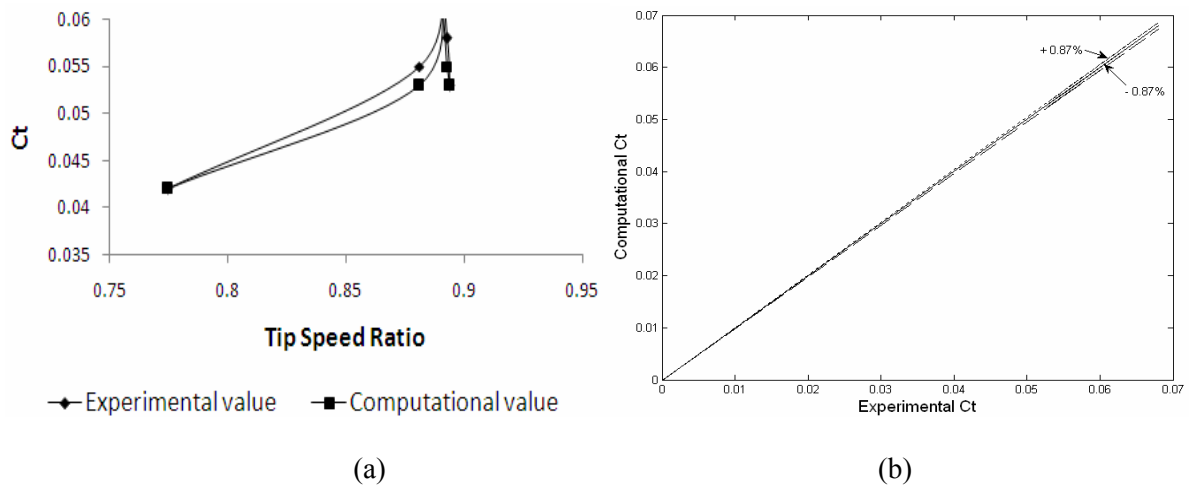


Figure 19. (a) Variation of C_t with TSR, and (b) deviation of computational C_t from experimental C_p for H/D ratio 1.80

From Figures 6 and 7, it is found that, for H/D ratio 0.85, the maximum C_p obtained is 0.232 at a TSR of 2.124, and the maximum C_t obtained is 0.116 at a TSR of 1.692. And for this H/D ratio, the standard deviation of computational C_p from experimental C_p is 1.57% and that of computational C_t from experimental C_t is 0.6%. From Figures 8 and 9, it is found that, for H/D ratio 1.0, the maximum C_p obtained is 0.265 at a TSR of 2.214, and the maximum C_t obtained is 0.124 at a TSR of 1.962. And the standard deviation of computational C_p from experimental C_p is 0.81% and that of computational C_t from experimental C_t is 0.53%. From Figures 10 and 11, it is found that, for H/D ratio 1.10, the maximum C_p obtained is 0.264 at a TSR of 2.277, and maximum C_t obtained is 0.119 at a TSR of 2.214; the standard deviations of C_p and C_t are 1.57% and 0.56% respectively. From Figures 12 and 13, it is found that, for H/D ratio 1.33, the maximum C_p obtained is 0.134 at a TSR of 1.085 and maximum C_t obtained is 0.124 at a TSR of 1.085 and the standard deviations of C_p and C_t are 0.59% and 0.51% respectively. From Figures 14 and 15, it is found that, for H/D ratio 1.54, the maximum C_p obtained is 0.097 at a TSR of 0.837 and maximum C_t obtained is 0.125 at a TSR of 0.837 and the standard deviations of C_p and C_t are 2.68% and 3.66% respectively. From Figures 16 and 17, it is found that, for H/D ratio 1.72, the maximum C_p obtained is 0.064 at a TSR of 0.792 and maximum C_t obtained is 0.081 at a TSR of 0.792 and the standard deviations of C_p and C_t are 1.29% and 1.59% respectively. From Figures 18 and 19, it is found that, for H/D ratio 1.80, the maximum C_p obtained is 0.59 at a TSR of 0.888 and maximum C_t obtained is 0.066 at a TSR of 0.888 and the standard deviations of C_p and C_t are 0.94% and 0.87% respectively.

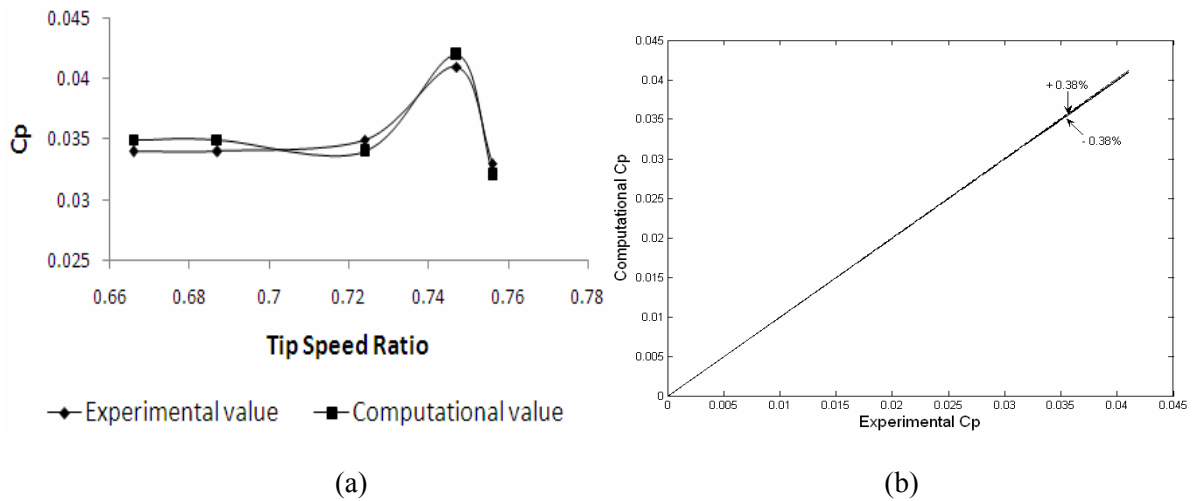


Figure 20. (a) Variation of C_p with TSR, and (b) deviation of computational C_p from experimental C_p for H/D ratio 1.92

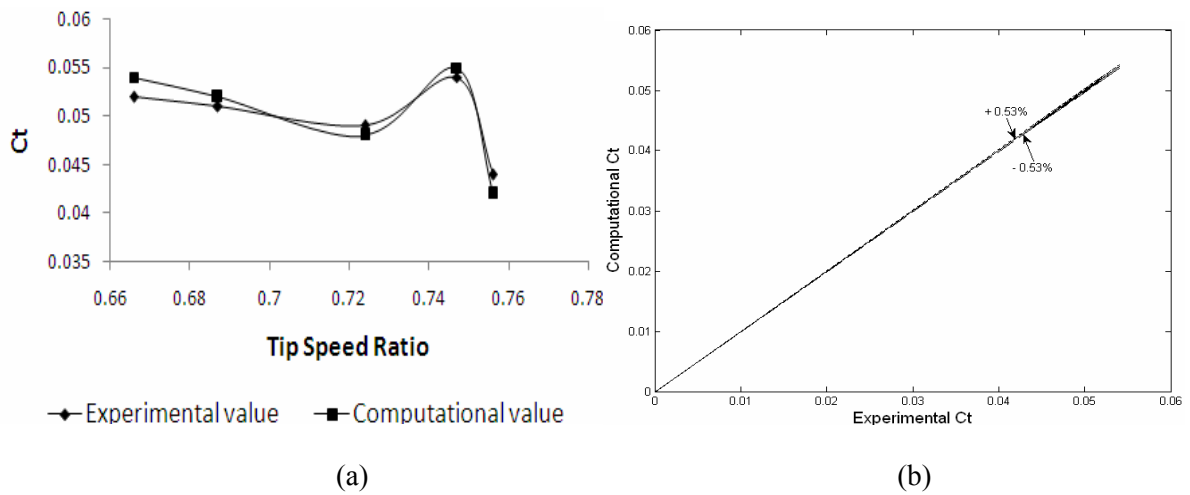


Figure 21. (a) Variation of C_t with TSR, and (b) deviation of computational C_t from experimental C_p for H/D ratio 1.92

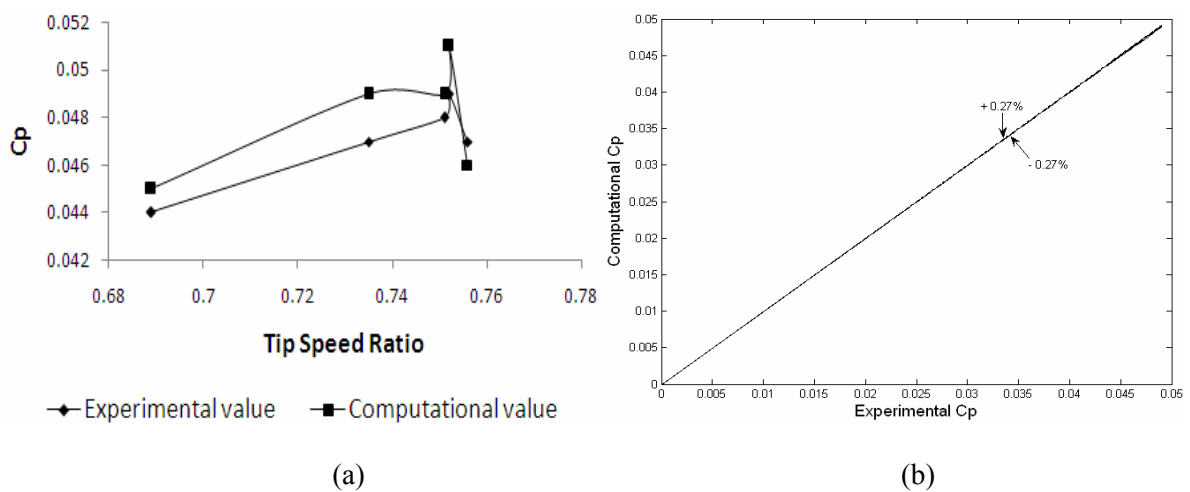


Figure 22. (a) Variation of C_p with TSR, and (b) deviation of computational C_p from experimental C_p for H/D ratio 2.10

From Figures 20 and 21, it is found that, for H/D ratio 1.92, the maximum C_p obtained is 0.042 at a TSR of 0.747 and maximum C_t obtained is 0.055 at a TSR of 0.747 and the standard deviations of C_p and C_t are 0.38% and 0.53%.

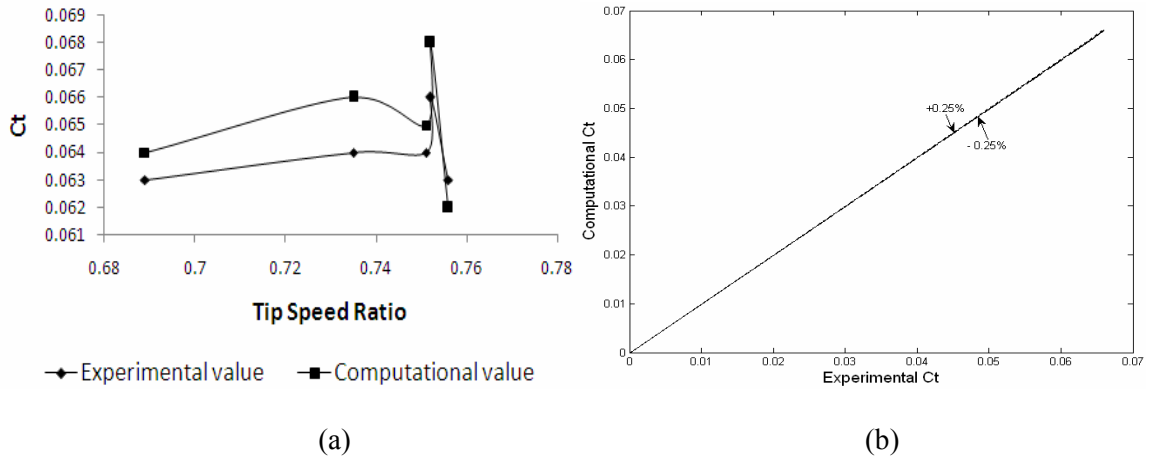


Figure 23. (a) Variation of C_t with TSR, and (b) deviation of computational C_t from experimental C_p for H/D ratio 2.10

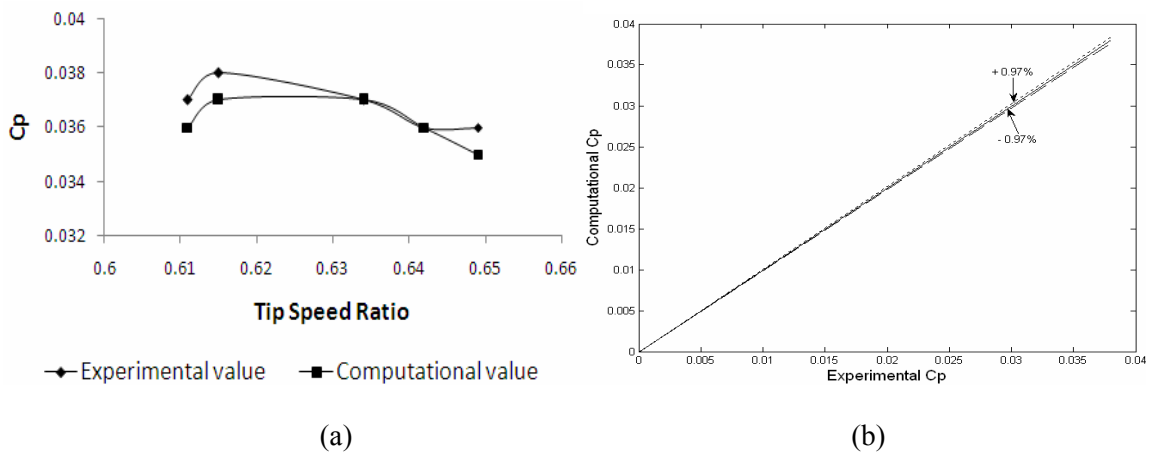


Figure 24. (a) Variation of C_p with TSR, and (b) deviation of computational C_p from experimental C_p for H/D ratio 2.20

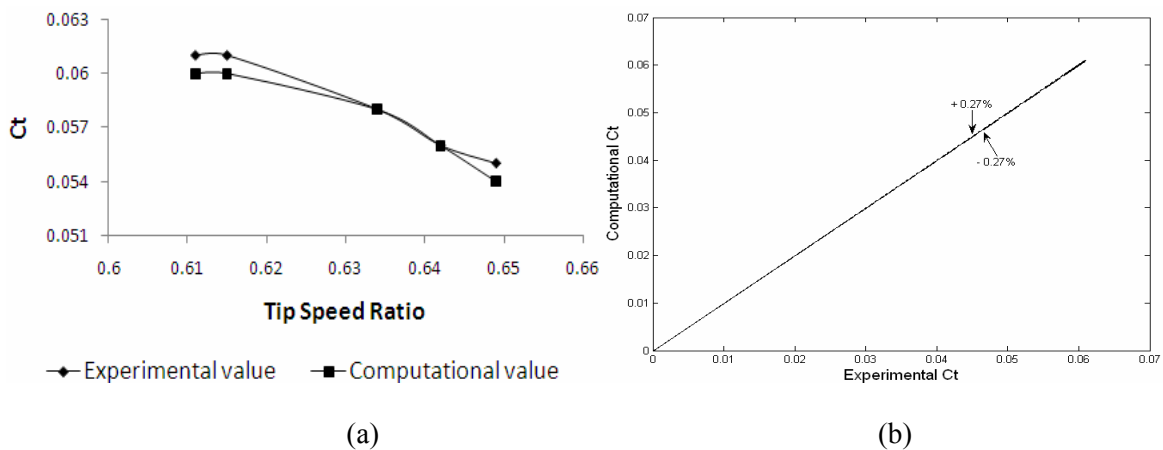


Figure 25. (a) Variation of C_t with TSR, (b) deviation of computational C_t from experimental C_p for H/D ratio 2.20

From Figures 22 and 23, it is found that for H/D ratio 2.10, the maximum C_p obtained is 0.051 at a TSR of 0.752 and maximum C_t obtained is 0.068 at a TSR of 0.752 and the standard deviations of C_p and C_t are 0.27% and 0.25% respectively. From Figures 24 and 25, it is found that, for H/D ratio 2.20, the maximum C_p obtained is 0.056 at a TSR of 0.642 and maximum C_t obtained is 0.06 at a TSR of 0.615 and the standard deviations of C_p and C_t are 0.97% and 0.27% respectively.

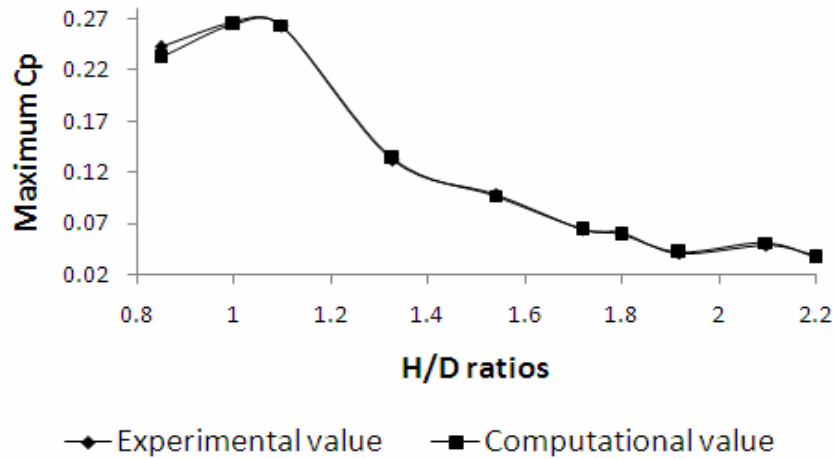


Figure 26. Variation of experimental maximum C_p from computational maximum C_p at different H/D ratios

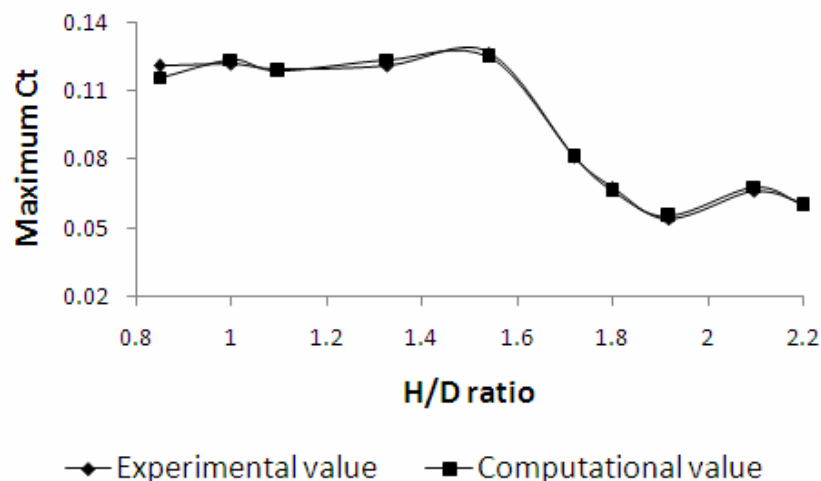
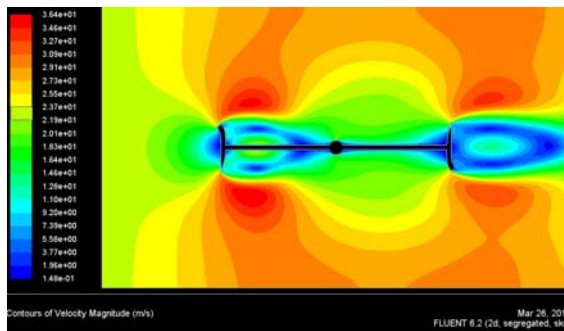


Figure 27. Variation of experimental maximum C_t from computational maximum C_t at different H/D ratios

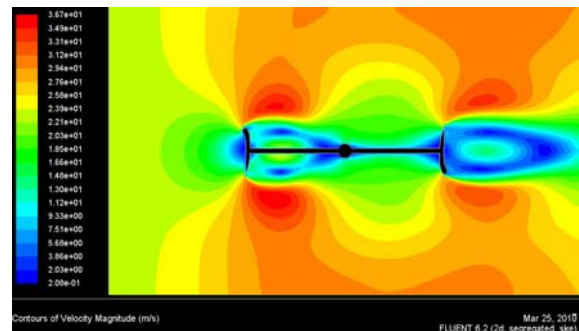
Figure 26 shows the comparison of the variations of computational and experimental maximum C_p values for each H/D ratio, whereas Figure 27 shows the comparison of the variations of computational and experimental maximum C_t values for each H/D ratio. These Figures show very good agreement between the computational and experimental results of C_p and C_t at all H/D ratios.

Figures 28 (a), (b), (c), (d), (e), and (f) show the velocity magnitude contours for the two-bladed rotor for ten H/D ratios, namely 0.85, 1.0, 1.10, 1.33, 1.72 & 1.92. The velocity contours show that the flow is accelerated while passing over the rotor blades. The velocity at the blade tips is almost 1.6 times higher compared to the input velocity on the extreme left of the computational domain. This velocity difference is responsible for the power stroke of the blades during its clockwise rotation. Wind turbines have the ability to produce highest aerodynamic torque at blade tips. And high velocity magnitude at the blade tips ensures augmentation in aerodynamic torque production. Further, the velocity contours show that, with the increase of H/D ratio, the velocity magnitude difference from inlet up to the rotor increases up to a certain H/D ratio and then decreases meaning loss of performance for the turbine with increase of H/D

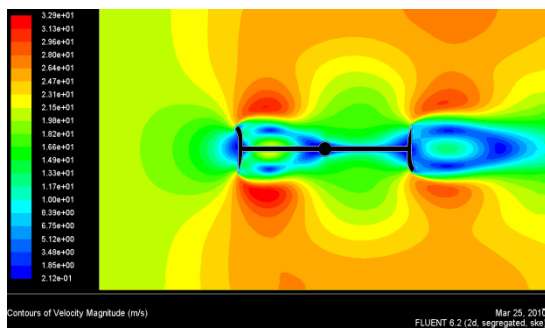
ratio. For example at H/D ratio of 0.85, the maximum velocity is 36.4 m/s with a inlet velocity of 23.291 m/s and for H/D ratio of 1.0, the maximum velocity is 36.7 m/s with a inlet velocity of 23.291 m/s . But after it, as the H/D ratio increases there is a fall in velocity magnitude difference. For example, for H/D ratio of 1.10, 1.33, 1.72, 1.92 the maximum velocities are 32.9 m/s, 31 m/s 28.4 m/s and 26.2 m/s respectively.



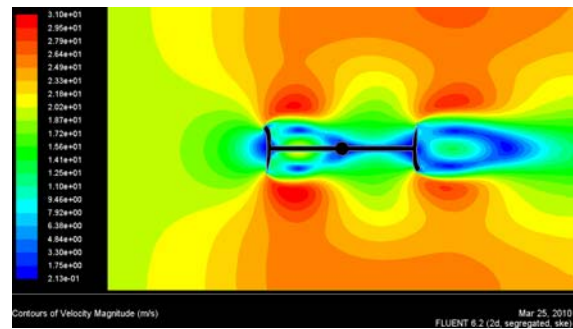
(a) H/D = 0.85



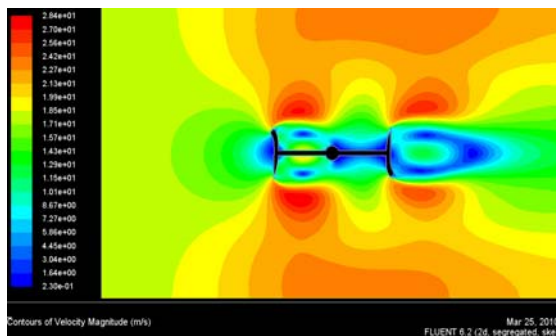
(b) H/D = 1.0



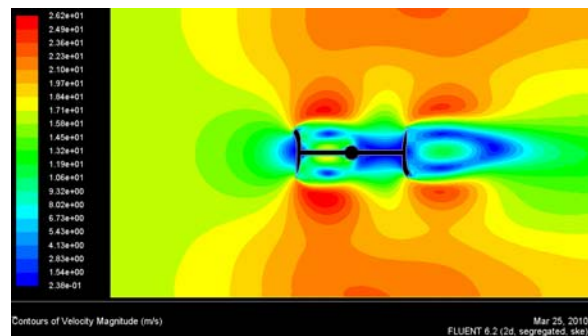
(c) H/D = 1.10



(d) H/D = 1.33



(e) H/D = 1.72



(f) H/D = 1.92

Figure 28. Velocity magnitude contours for H/D ratios: (a) 0.85, (b) 1.0, (c) 1.10, (d) 1.33, (e) 1.72, (f) 1.92

5. Conclusions

The power coefficients and torque coefficients of the turbine were evaluated from the CFD analysis for ten different H/D ratios, and the results were compared with the experimental results for the turbine. It was found that there was a close agreement between the computational and experimental results. The deviation of computational C_p from experimental C_p was within $\pm 2.68\%$, whereas the deviation of computational C_t from experimental C_t was within $\pm 3.66\%$. These findings highlight the potential of CFD as a tool for the performance measurement of vertical axis wind rotor. Further, the contour plots of velocity magnitude were generated for the rotor for each H/D ratio. From the contour plot analysis, it is observed that velocity at the blade tips is almost 1.6 times higher compared to the input velocity.

Moreover, with the increase of H/D ratio, the velocity magnitude difference from inlet up to the rotor increases upto H/D ratio 1.0 and then decreases meaning loss of performance for the turbine with increase of H/D ratio. It can be concluded that the velocity difference from inlet up to the rotor is responsible for the power stroke of the blades during its clockwise rotation. Future study could entail 3D wake modeling of the rotor to study dynamic nature of the separated vortices along with their effect on lift generated for such rotor.

References

- [1] Fernando L. Ponta, Pablo M. Jacovkis, A vortex model for Darrieus turbine using finite element techniques, *Journal of Renewable Energy*, pp 1–18, vol.24, 2001.
- [2] Darrieus G.J.M, Turbine having its rotating shaft transverse to the flow of the current, US Patent no. 1.835.018, 1931.
- [3] Islam, M., Esfahanian, V., D.S-K, Ting., & Fartaj, A.: Applications of Vertical Axis Wind Turbines for Remote Areas. In: Proceedings of 5th Iran National Energy Conference, Tehran, Iran, Spring 2005.
- [4] Bach. G, Investigation Concerning Savonius rotors and related Machines, Translate into English by Brace Research Institute.,Quebec,Canada,1931.
- [5] Macpherson. R B , Design ,Development and testing of Low Head High Efficiency Kinetic Energy Machine, M.Sc Thesis,University of Massachusetts,Amherst,M.A.1972.
- [6] Newman B.G, Measurement on a Savonius rotor with variable gap, Proceeding of Sherbrook University Symposium on wind energy, Sherbrook Canada, pp-116, 1974.
- [7] Khan M.H, Improvement of Savonius Rotor-windmill, M.S. thesis, University of the Philippines, Lasbonas, 1975.
- [8] Modi V.J., Optimal configuration studies and prototype design of a wind energy operated irrigation system, *Journal of Wind Engineering & Industrial Aerodynamics*, Vol. 16, pp 85-96, 1984.
- [9] Sharma K.K, Gupta R, Singh S. K and Singh S. R, Experimental investigation of the characteristics of a Savonius wind turbine, *Journal of Wind Engineering*, Vol. 29 issue 1 pp 77-82, 2005.
- [10] Biswas A, Gupta R, Sharma K. K, Experimental Investigation of Overlap and Blockage Effects on Three-Bucket Savonius Rotors, *Journal of Wind Engineering*, Vol. 31, No. 5, pp 363–368, 2007.
- [11] Howell, R., Qin ,N., Edwards, J., Durrani, N.: Wind tunnel and numerical study of a small vertical axis wind turbine. *Renewable Energy Journal*, 35, 412-422 (2010).
- [12] Gupta, R. Das, R. Sharma, K.K., Experimental study of a Savonius-Darrieus wind machine, Proceedings of the International Conference on Renewable Energy for Developing Countries-2006.
- [13] Gupta, R, Biswas, A. Sharma K.K., CFD analysis of a combined three bucket Savonius and three bucket Darrieus rotor at various overlap conditions, *Journal of Renewable and Sustainable Energy*, 2009.



Rajat Gupta was born on 10th July 1959. . He has done Ph.D. from Indian Institute of Technology; Delhi, India, in the year 1995. He has been a Professor since 1996.

More than 85 papers of his have been published in National/International Journals/Conferences. He is presently holding the post of Dean (Sponsored Research and Consultancy) in N.I.T Silchar. His research interest is in the field of fluid dynamics and its application, wind energy.

E-mail address: r_guptanitsil@yahoo.com



Sukanta Roy is an M.Tech student in Thermal Engineering from NIT, Silchar, working under the guidance of Prof. Rajat Gupta.

His area of interest is in the field of fluid dynamics and its application, wind energy.

E-mail address: sukantamech07@gmail.com



Agnimitra Biswas is a PhD student from NIT, Silchar, working under the guidance of Prof. Rajat Gupta.

He has done his M.Tech in Thermal Engineering from NIT, Silchar, India in the year of 2007.

His area of interest is in the field of wind energy.

E-mail address: agnibis@yahoo.co.in